

Article

Desilicated ZSM-5 Zeolites for the Production of Renewable *p*-Xylene via Diels–Alder Cycloaddition of Dimethylfuran and Ethylene

Joel McGlone , Peter Prielcel , Luigi Da Vià , Liqaa Majdal and Jose A. Lopez-Sanchez * 

Stephenson Institute for Renewable Energy, Department of Chemistry, University of Liverpool, Liverpool L69 7ZD, UK; jomcgl1@hotmail.com (J.M.); peter.prielcel@liverpool.ac.uk (P.P.); davia.luigi@gmail.com (L.D.V.); L.I.Majdal@liverpool.ac.uk (L.M.)

* Correspondence: jals@liverpool.ac.uk; Tel.: +44-151-79-43535

Received: 30 April 2018; Accepted: 14 June 2018; Published: 20 June 2018



Abstract: The selective production of *p*-xylene and other aromatics starting from sugars and bioderived ethylene offers great promise and can eliminate the need for separation of xylene isomers, as well as decreasing dependency on fossil resources and CO₂ emissions. Although the reaction is known, the microporosity of traditional commercial zeolites appears to be a limiting factor. In this work, we demonstrate for the first time that simply desilication of microporous commercial zeolites by a simple NaOH treatment can greatly enhance conversion and selectivity. The [4 + 2] Diels–Alder cycloaddition of 2,5-dimethylfuran with ethylene in a pressurised reactor was investigated using a series of H-ZSM-5 catalysts with SiO₂/Al₂O₃ ratios 30 and 80 with increasing pore size induced by desilication. X-ray diffraction, scanning electron microscopy, ²⁷Al magic-angle spinning nuclear magnetic resonance, temperature programmed desorption of ammonia, and nitrogen physisorption measurements were used to characterise the catalysts. The enhancement of conversion was observed for all desilicated samples compared to the untreated zeolite, and increases in temperature and ethylene pressure significantly improved both dimethylfuran conversion and selectivity to *p*-xylene due to the easier desorption from the zeolite's surface and the augmented cycloaddition rate, respectively. A compromise between acidity and mesoporosity was found to be the key to enhancing the activity and maximising the selectivity in the production of *p*-xylene from 2,5-dimethylfuran.

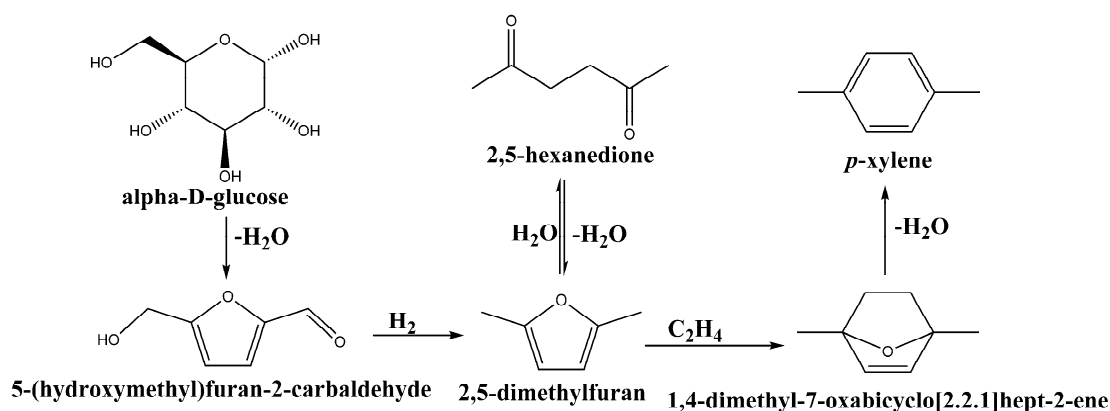
Keywords: renewable *p*-xylene; Diels–Alder; desilication; dimethylfuran; biomass; ZSM-5; hierarchical zeolites; renewable aromatics

1. Introduction

Due to diminishing quantities of fossil fuels, lignocellulosic biomass is attracting more attention as a feedstock for platform chemicals due to its large availability and economic factors [1]. One of these platform chemicals obtainable from biomass is *p*-xylene [2,3], a precursor in the terephthalic acid synthesis, which can be polymerised to produce polyethylene terephthalate (PET). *p*-Xylene is currently produced on an industrial scale from the catalytic reforming of petroleum naphtha, which is part of the benzene-toluene-xylene (BTX) fraction. Current market demand for *p*-xylene is typically around 34% of the BTX fraction [4].

Brion et al. [5] found that furan ring compounds could be converted into a six-membered ring via cycloaddition to produce an oxa-norbornene intermediate followed by β elimination (Scheme 1). Recent studies have shown that 2,5-dimethylfuran (DMF) could act as a potential feedstock for the production of *p*-xylene [6–10]. The advantage of this route is the production of the pure para isomer of xylene, thus removing the necessity of purifying *p*-xylene, as is the case in its production from

fossil sources. DMF itself can be produced from glucose in a two-step process. Glucose can be converted into 2,5-hydroxymethylfurfural (HMF), which can then be hydrodeoxygenated to produce DMF (Scheme 1) [11].



Scheme 1. Proposed reaction for the conversion of glucose to *p*-xylene.

The production of *p*-xylene was reported via the Diels–Alder cycloaddition of DMF and ethylene over different acid catalysts, such as zeolite FAU (faujasite) [6,12,13], γ -alumina, niobic acid, H-FAU (ZSM-5) [14], or zeolite BEA (beta) [9,15,16]. H-BEA was shown to be almost an order of magnitude more active than γ -alumina, niobic acid, or H-ZSM-5. It was recently discussed that both Brønsted and Lewis acids are very effective in catalysing Diels–Alder cycloaddition [3], and several teams demonstrated enhancement in catalytic activity of zeolites containing both Brønsted and Lewis acid sites [9,17,18]. Additionally, it was shown that polar aprotic solvent, such as 1,4-dioxane, improves both DMF conversion and *p*-xylene yield attributable to the increased dehydration rate. Several studies were dedicated to the detailed study of the reaction mechanism and regimes reflecting different rate-limiting steps and thermodynamics [6,7,12,13,16,19]. It was found that regimes of high and low acid concentration differ significantly and result in switching the rate-limiting step from the Diels–Alder cycloaddition to the dehydration of oxanorbornene, respectively.

It was reported that inducing mesoporosity in zeolites (producing hierarchical zeolites) can alleviate diffusion limitations and significantly increase catalytic activity in a variety of reactions [14,20]. It has been argued that the secondary porosity could also be used to store coke and therefore avoid blockage of the active microporous sites [21]. One of the ways to introduce mesoporosity in zeolites is the removal of framework Si atoms (desilication) [22]. Dean [23] first suggested the idea of alkaline treatment for zeolites to increase performance in the mordenite in the gas–oil reaction and noted that crystallinity was preserved with a three times higher conversion compared to the untreated parent zeolite. Groen et al. [22] found that desilication preserved crystallinity and Brønsted acidity of the parent zeolite.

In view of this, we decided to produce hierarchical zeolites for the Diels–Alder cycloaddition of ethylene to DMF with the hope that increasing pore size would facilitate mass transport phenomena and increase reaction rates. In this paper, we investigate the effect of increasing the pore size of ZSM-5 catalysts with differing SiO₂/Al₂O₃ ratios by alkaline treatment and how this affects the structural properties of the ZSM-5, as well as how beneficial this can be for the production of renewable aromatics *p*-xylene.

2. Results and Discussion

2.1. X-ray Diffraction

XRD patterns of the untreated and alkaline-treated samples were obtained and are shown in Figures 1 and 2 for Z30 and Z80, respectively. All samples show diffractions of ZSM-5 based on JCPDS

PDF 01-080-0922. The parent zeolite was compared to the alkaline-treated ones, and intensity of the (101) peak was used for the crystallinity calculation.

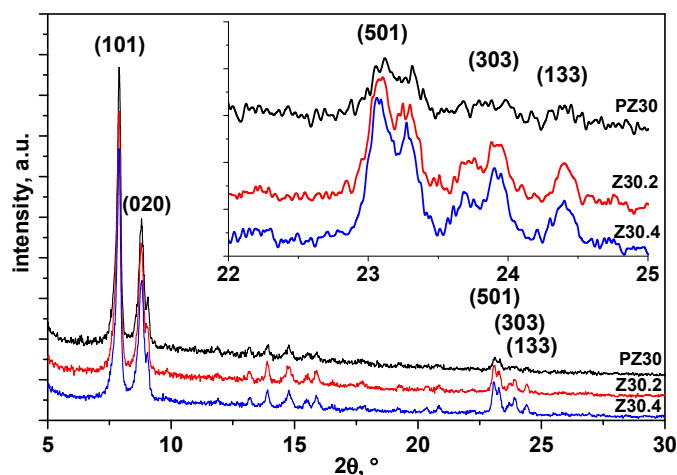


Figure 1. XRD patterns of PZ30 (top, black), Z30.2 (middle, red), and Z30.2 (bottom, blue).

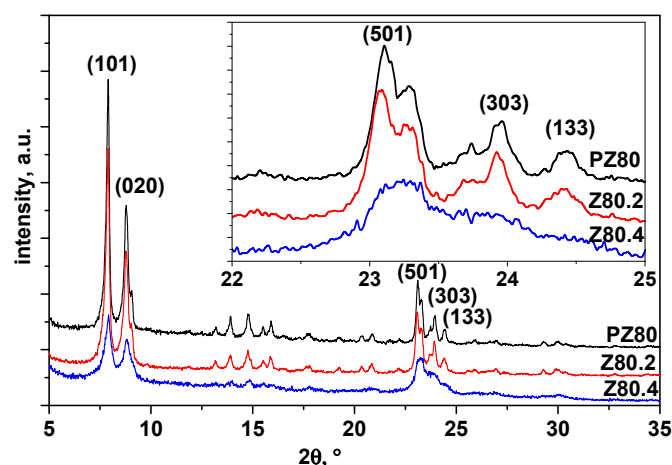


Figure 2. XRD patterns of PZ80 (top, black), Z80.2 (middle, red), and Z80.2 (bottom, blue).

It was found that 0.2 M NaOH treatments of PZ30 and PZ80 did not significantly reduce the material crystallinity. Alkaline treatment of Z30 (up to 0.4 M NaOH) preserved crystallinity up to 87% of the original zeolite, as evidenced by the presence of diffraction lines (101), (020), and (501), which are typical of ZSM-5 diffraction patterns (Figure 1).

On the other hand, the alkaline treatment of PZ80 with 0.4 M NaOH significantly reduced the zeolite crystallinity down to 31% of the original value (Figure 2). These results are in agreement with the hypothesis of Verboekend et al. [24], who claimed that desilication is more difficult at lower $\text{SiO}_2/\text{Al}_2\text{O}_3$ ratios due to the repulsion by the negative charge on the framework aluminium ions and would be easier with $\text{SiO}_2/\text{Al}_2\text{O}_3$ ratios >50 due to uncontrolled desilication.

2.2. Surface Area and Porosity of the Materials

N_2 isotherms of PZ30 and PZ80 display typical type I isotherm with a plateau at a higher relative pressure according to IUPAC (International Union of Pure and Applied Chemistry) classification (Figures 3 and 4).

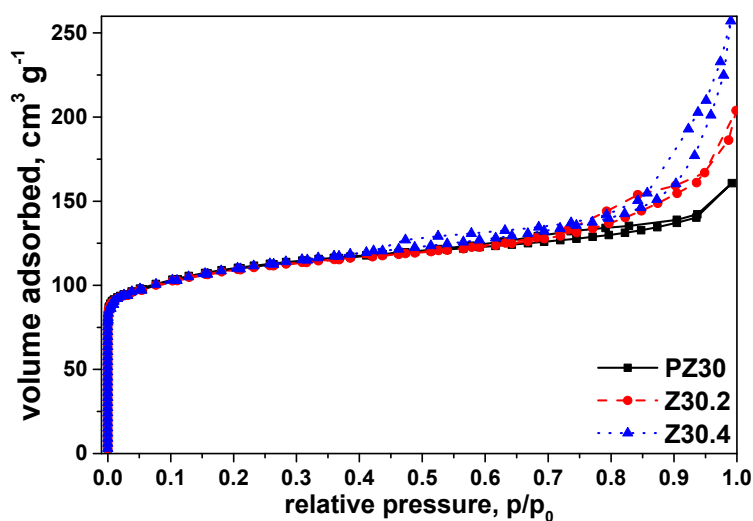


Figure 3. N₂ isotherms of PZ30 (black square, full line), Z30.2 (red circle, dashed line), and Z30.4 (blue triangle, dotted line) at 77 K.

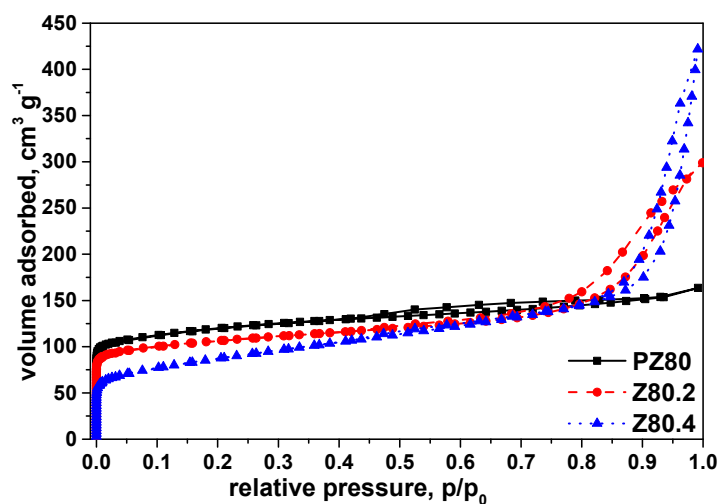


Figure 4. N₂ isotherms of PZ80 (black square, full line), Z80.2 (red circle, dashed line), and Z80.4 (blue triangle, dotted line) at 77 K.

In addition to this, both PZ30 and PZ80 exhibit a small hysteresis, which is indicative of limited mesoporosity. The shapes of the isotherms confirm that the structure of PZ30 and PZ80 is dominated by microporosity. N₂ isotherms of all alkaline-treated Z30 and Z80 show a combination of type I and type IV isotherms with an increased uptake of N₂ and pronounced hysteresis, which is indicative of increased mesoporosity. Brunauer–Emmett–Teller (BET) measurements showed that alkaline treatment had minimal effect on the surface area of Z30 (Table 1).

Table 1. Physical properties of untreated and treated H-ZSM-5 Z30 and Z80 catalysts.

Catalyst	S_{Bet} ($\text{m}^2 \text{g}^{-1}$) ^a	V_{total} ^b ($\text{cm}^3 \text{g}^{-1}$)	V_{micro} ^c ($\text{cm}^3 \text{g}^{-1}$)	S_{meso} ^c ($\text{m}^2 \text{g}^{-1}$)	Crystallinity (%) ^d	$\text{SiO}_2/\text{Al}_2\text{O}_3$ Ratio ^e	Total Acid Sites, $\mu\text{mol g}^{-1}$ ^f	Weak Acid Sites, $\mu\text{mol g}^{-1}$ ^f	Strong Acid Sites, $\mu\text{mol g}^{-1}$ ^f	Brønsted Acid Sites, $\mu\text{mol g}^{-1}$ ^g	Lewis Acid Sites, $\mu\text{mol g}^{-1}$ ^g
PZ30	344	0.250	0.147	142	100	28	581	165	416	295	286
Z30.2	340	0.315	0.147	181	92	24	655	205	450	163	492
Z30.4	340	0.397	0.148	216	87	21	692	266	426	337	355
PZ80	376	0.253	0.165	131	100	72	333	55	278	166	167
Z80.2	327	0.454	0.143	224	84	50	369	109	260	24	345
Z80.4	312	0.734	0.122	260	31	31	504	260	244	368	136

^a Brunauer–Emmett–Teller (BET) method; ^b $P/P_0 = 0.99$; ^c NLDFT (non-local density functional theory); ^d measured by XRD; ^e ICP-OES (inductively coupled plasma-optical emission spectroscopy); ^f NH_3 -TPD; ^g B/L (Brønsted/ Lewis) acid site ratio from pyridine FTIR and to total amount from TPD (temperature programmed desorption).

Upon the treatment with 0.2 M and 0.4 M NaOH, the mesopore surface area of Z30 increased from 142 to 181 and 216 $\text{m}^2 \text{g}^{-1}$ compared to the parent zeolite, while the micropore volume was preserved.

In the case of Z80, N_2 adsorption measurements showed that both the surface area and microporosity decreased after the NaOH treatment. The BET surface area decreased from 376 to 312 $\text{m}^2 \text{g}^{-1}$ and the volume of micropores from 0.165 to 0.122 $\text{cm}^3 \text{g}^{-1}$ for Z80.4 when compared to the untreated PZ80. The alkaline treatment also had a profound effect on the mesopore surface area, which increased from 131 (PZ80) to 260 $\text{m}^2 \text{g}^{-1}$ (Z80.4). These porosity changes in both Z30 and Z80 further corroborate the difference in difficult desilication at lower $\text{SiO}_2/\text{Al}_2\text{O}_3$ ratios and uncontrolled desilication at $\text{SiO}_2/\text{Al}_2\text{O}_3$ 80 [24].

2.3. Acidity Measurements

There were two desorption peaks in ammonia TPD (temperature programmed desorption) profiles (Figures S1 and S2). The first desorption peak at $\sim 225^\circ\text{C}$ corresponds to the weak (Lewis) acid sites, whereas the second desorption peak at $\sim 385^\circ\text{C}$ corresponds to the strong (both Brønsted and Lewis) acid sites [25,26]. It was reported that the concentration of the weakly bound ammonia observed at the low temperature peak has no catalytic importance, and it was demonstrated that it can be decreased by extending the flushing time with the inert gas [27].

The total acidity values of both the parent PZ30 and PZ80 are in agreement with the data present in the literature [27,28]. Both Z30 and Z80 desilicated samples showed increases in the total acidity, which is in agreement with the decrease in the $\text{SiO}_2/\text{Al}_2\text{O}_3$ ratio after the alkaline treatment; although, these results contradict the findings of Rac et al. [28], who found a decrease in the total acidity of all desilicated samples when compared to their corresponding parent. This could be due to the fact that during the desilication, the intensities of both the low and high temperature peaks increase. Also, Rac and co-workers used calorimetry compared to the TPD used in this study.

In the case of the parent PZ30 with a low $\text{SiO}_2/\text{Al}_2\text{O}_3$ ratio, the rigid zeolite structure and close proximity of the framework Si and Al (Lowenstein's rule) prevents the facile desilication to some extent, and the change in acidity profile is the least significant. This is also documented by the decrease in the $\text{SiO}_2/\text{Al}_2\text{O}_3$ ratio from 28 (PZ30) to 24 (Z30.2) and 21 (Z30.4) and the low decrease in crystallinity ($<15\%$). As shown in Table 1, the total acidity for the Z30.2 and Z30.4 increased from 581 to 655 and 692 $\mu\text{mol g}^{-1}$, respectively. The most pronounced change in the acidity profile was found to come from the weak acid sites, which could be due to the increased mesoporosity, as it was suggested by Rodriguez-Gonzalez et al. [27] that weakly bound NH_3 can physisorb onto itself within the pores. The number of strong acid sites was not affected significantly and increased slightly for treated samples by max. 8% of the parent value, which is in good agreement with literature [25].

2.4. Microscopy

SEM measurements showed PZ30 and PZ80 displayed well-defined morphologies of compact particle sizes ca. 250 nm. The alkaline treatment with sodium hydroxide had contrasting effects on the morphologies of PZ30 and PZ80 (Figure 5). The external surfaces remained largely intact upon mild treatment with sodium hydroxide. This suggests that silicon extraction did not largely take place on the external surface of the zeolite crystals. Similar conclusions were reported by Sadowaska et al. [29]. Alkaline treatment had minimal effect on the morphology of PZ30, whereas for PZ80, there was a clear change in the morphology of the crystal structure after the alkaline treatment, as can be seen from the formation of a less compact structure (more images in Supplementary Information Figures S3 and S4). In detail, the transition from PZ30 to Z30.2 did not show significant changes in the shape of the crystallites, nor separation of the smaller crystals. In the case of Z80, the division of large crystallites into smaller bulks is clearly visible.

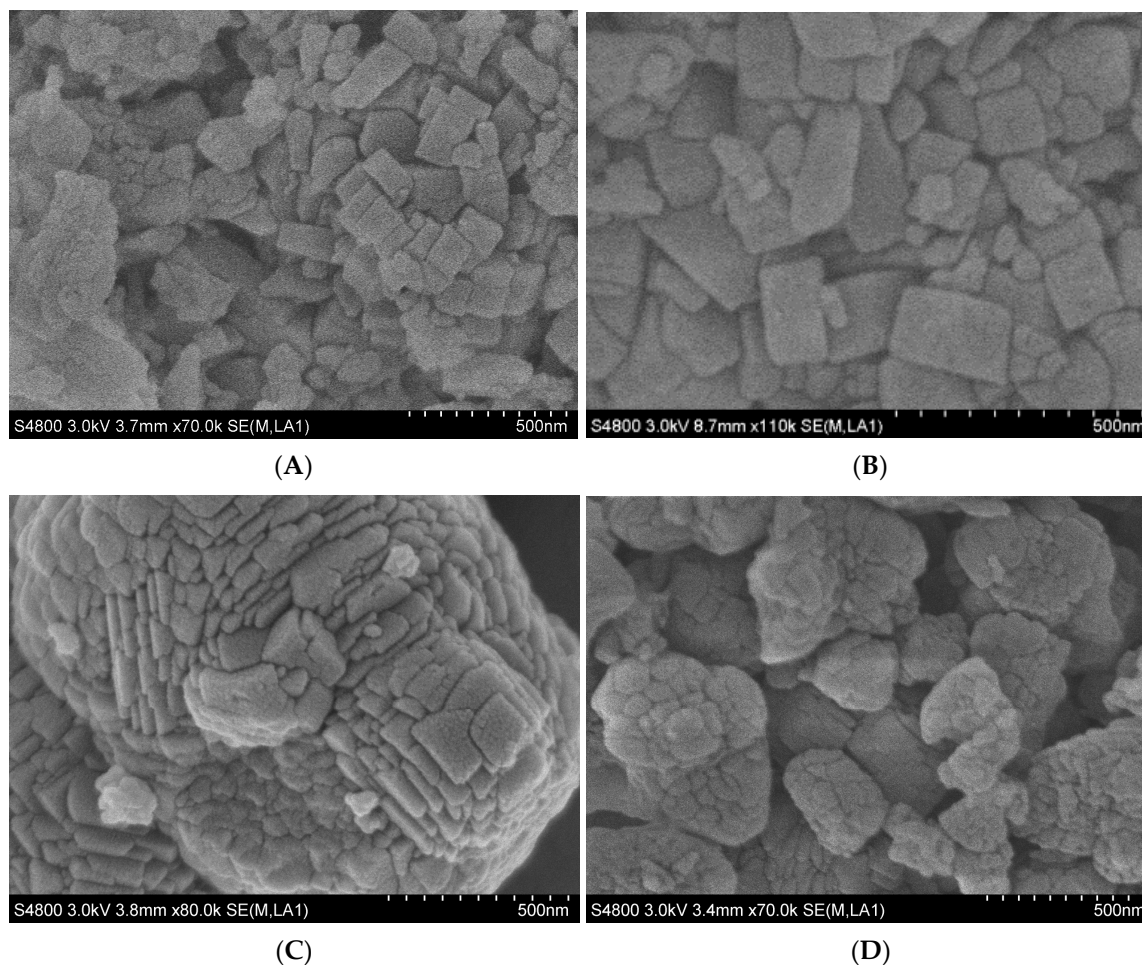


Figure 5. SEM images of untreated and treated HZSM-5. PZ30 (A); Z30.2 (B); PZ80 (C); and Z80.2 (D).

2.5. ^{27}Al MAS NMR

^{27}Al MAS NMR (magic angle spinning nuclear magnetic resonance) measurements were performed to determine the coordination of aluminium in the presented zeolite samples before and after the desilication treatment (Figure 6). The NMR spectra show peaks centred at ca. 54, 45–35, and 0 ppm, which correspond to framework aluminium in tetrahedral coordination (Al_{Td}) and extra-framework penta-coordinated and octahedral aluminium (Al_{Oh}), respectively [30].

As expected, the majority of Al occupies tetrahedral framework positions (Table 2). It can be seen that in both cases of Z30 and Z80, the isotropic shift of the 54 ppm resonance is widened as the concentration of the desilication agent is increased, which indicates the change of T-O-T angles in the framework (T is either Al or Si) [31]. This effect was more pronounced in the case of Z80, which agreed with its easier desilication and more pronounced decrease in $\text{SiO}_2/\text{Al}_2\text{O}_3$ ratio and crystallinity.

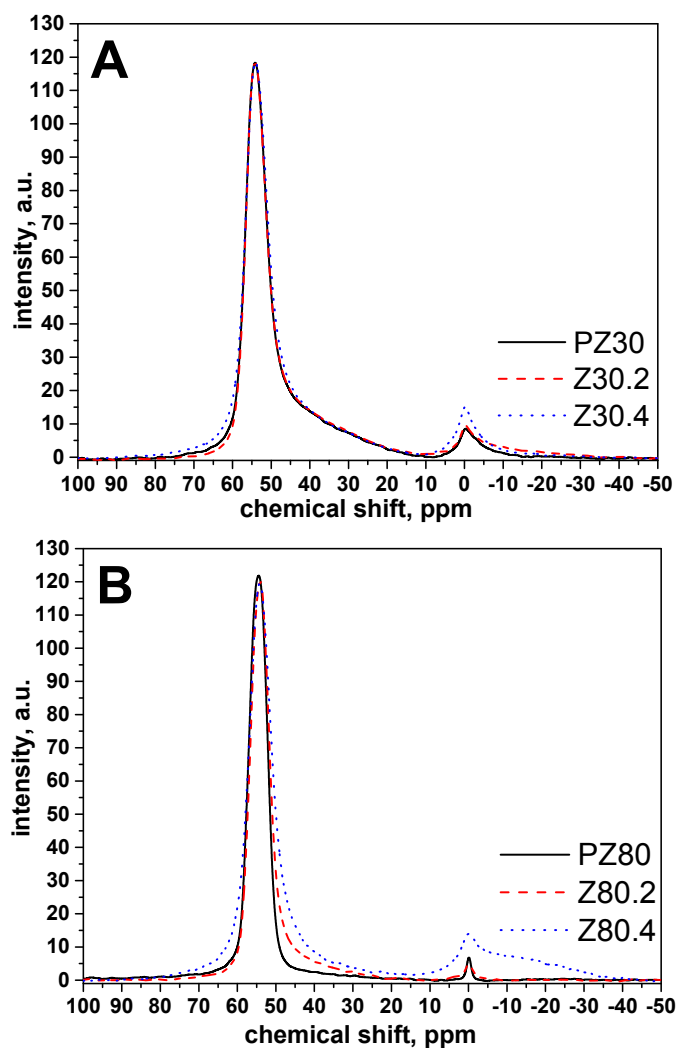


Figure 6. ^{27}Al MAS NMR spectra of presented zeolites with $\text{SiO}_2/\text{Al}_2\text{O}_3$ ratios 30 (Z30) (A) and 80 (Z80) (B) before (PZ30, PZ80) and after the desilication treatment (Z30.2, Z30.4, Z80.2, Z80.4).

Table 2. Normalised areas and ratios of peaks at 54 and 0 ppm corresponding to framework and extra-framework aluminium.

SAMPLE	Ratio of Peaks at 54 to 0 ppm	Normalised Areas at Peak Positions	
		54 ppm	0 ppm
PZ30	17.8	0.947	0.053
Z30.2	11.9	0.923	0.077
Z30.4	11.1	0.917	0.083
PZ80	63.7	0.985	0.015
Z80.2	42.5	0.977	0.023
Z80.4	4.7	0.823	0.177

A similar effect to that of framework aluminium was observed in the case of extra-framework Al in octahedral coordination. As the concentration of NaOH during the desilication increased, so did the amount of extra-framework aluminium. Moreover, the widening of the peak at ca. 0 ppm indicates a broader distribution of the local extra-framework Al environment, which was again more pronounced in the case of Z80.

Worth noting is the possible presence of penta-coordinated extra-framework aluminium, which could be suggested by the presence of the shoulder at 45–35 ppm. In our case, the relative amount of this type of Al does not seem to change during the treatment of Z30 but slowly increases along with the increment of Al_{OH} .

2.6. Catalytic Activity

2.6.1. General Considerations and Conversion

As shown in Scheme 1, *p*-xylene is formed by the [4 + 2] cycloaddition of DMF with ethylene to form 7-oxabicyclo[2.2.1]hept-2-ene, which is dehydrated to form *p*-xylene. DMF can be also hydrolysed to form 2,5-hexanedione (HDO), which was shown to be able to dehydrate back to DMF and, according to this mechanism, could still be converted to *p*-xylene [12]. Trace amounts of 3-methyl-2-cyclopentenone (MCP) were found due to the intramolecular aldol reaction of 2,5-hexanedione. 1-ethyl-2,5-dimethylbenzene, which was found to be a product in the literature [6], was not found in our study. The reaction in which no catalyst was used yielded less than 3% conversion of DMF with no selectivity to any of the identified products. A typical time-dependent profile of the conversion of DMF and selectivities to the identified products is presented in Figure 7.

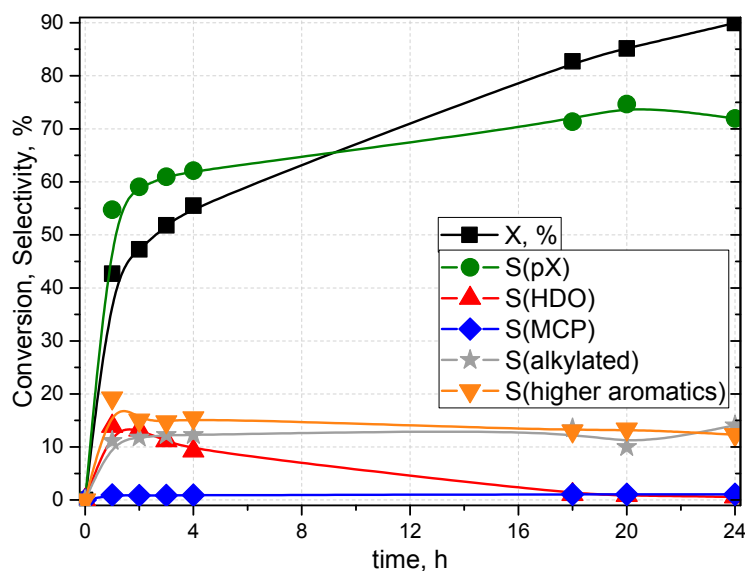


Figure 7. Conversion and selectivities to known products as a function of time for the Diels–Alder cycloaddition of 2,5-dimethylfuran (DMF) and ethylene over H-ZSM-5 (30). Reaction conditions: temperature, 250 °C; pressure, 55 bar; catalyst, 120 mg; 30 mL of 3 M DMF in *n*-octane; and stirring, 1100 rpm. Mass balance increased from 66% at first sampling to 73% at the end of the reaction.

As conversion of 2,5-dimethylfuran increases, *p*-xylene is produced, and its selectivity increase follows conversion until the last point, when it decreases slightly in favour of alkylated products. The selectivities to alkylated products, consisting of DMF and aromatics and higher aromatics with multiple aromatic rings, show an initial increase to ca. 10–15% after which they keep slightly decreasing until the end of the reaction. As mentioned before, hexanedione is produced but is again consumed, which suggests conversion back to DMF to produce *p*-xylene.

Conversion for both Z30 and Z80 treated by 0.2 M NaOH increased from 19.3% and 21.3% to 36% and 37%, respectively (Figures 8 and 9, Table S1).

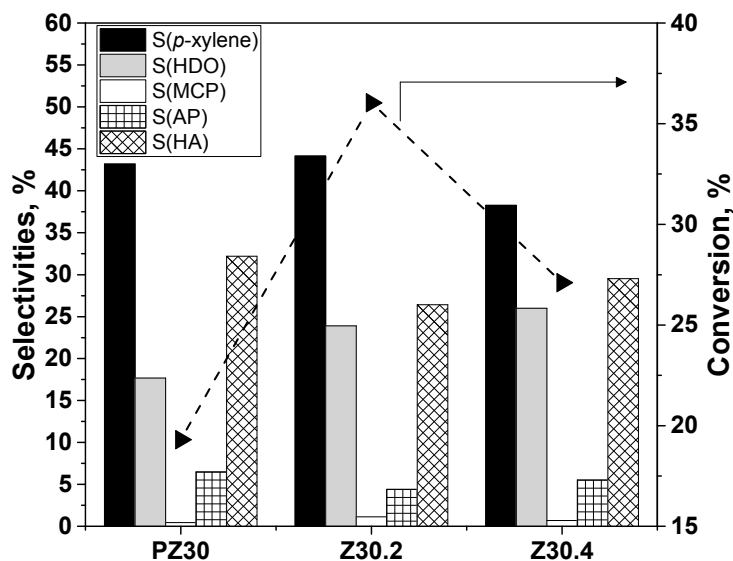


Figure 8. Conversion (X, symbol + line) and selectivity (S, columns) values for untreated and treated Z30. Conversion (triangle), S(*p*-xylene) (black), S(2,5-hexanedione) (HDO, grey), S(3-methyl-2-cyclopentenone) (MCP, white), S(alkylated products) (AP, square pattern), and S(higher aromatics) (HA, diagonal pattern). Reaction conditions: 180 °C, 40 bar total pressure (pressurised at 180 °C), 5.5 mL DMF, 0.45 mL tridecane (internal standard), 16.5 mL hexane, 110 mg catalyst, 20 h. The carbon mass balance was >96.5%, except in case of Z30.2 it was 85%.

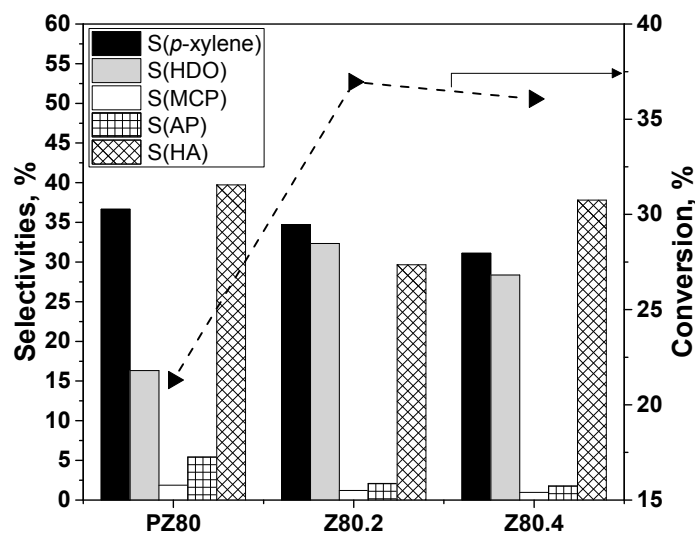


Figure 9. Conversion (X, symbol + line) and selectivity (S, columns) values for untreated and treated Z80. Conversion (triangle), S(*p*-xylene) (black), S(2,5-hexanedione) (HDO, grey), S(3-methyl-2-cyclopentenone) (MCP, white), S(alkylated products) (AP, square pattern) and S(higher aromatics) (HA, diagonal pattern). Reaction conditions: 180 °C, 40 bar total pressure (pressurised at 180 °C), 5.5 mL DMF, 0.45 mL tridecane (internal standard), 16.5 mL hexane, 110 mg catalyst, 20 h. The carbon mass balance was in all cases >94%.

This would suggest that increased porosity promotes the transformation of DMF to reaction products. However, the additional desilication and increase in the porosity for both Z30 and Z80 does not promote further the conversion when compared to the 0.2 M NaOH-treated samples. Nonetheless, the activity of the Z30.4 and Z80.4 increased to 27.1% and 36.1% when compared to the PZ30 and PZ80, respectively. As the effect of the alkaline treatment was more pronounced in the case of Z80, this

material was selected for the catalytic tests at high temperature. It can be seen that when the reaction temperature is increased to 250 °C, the DMF conversion for Z80.2 is significantly enhanced from 16% to 51% when compared to PZ80 (Figure 10) under the same conditions.

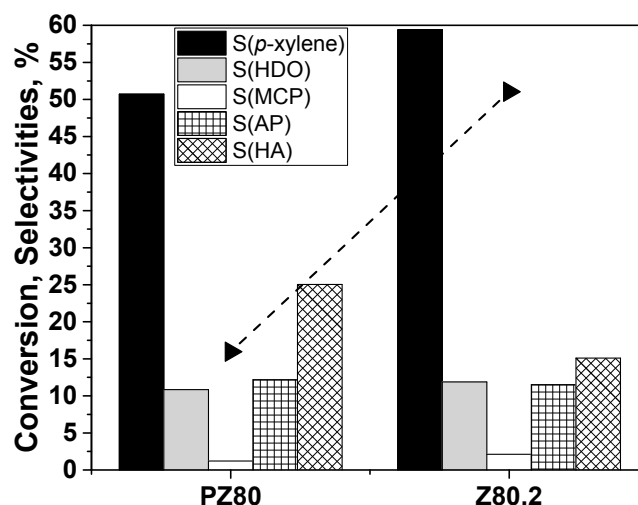


Figure 10. Conversion (X, symbol + line) and selectivity (S, columns) values for untreated PZ80 and treated Z80.4. Conversion (triangle), S(*p*-xylene) (black), S(2,5-hexanedione) (HDO, grey), S(3-methyl-2-cyclopentenone) (MCP, white), S(alkylated products) (AP, square pattern) and S(higher aromatics) (HA, diagonal pattern). Reaction conditions: 250 °C, 55 bar total pressure (pressurised at 250 °C), 5.5 mL DMF, 0.45 mL tridecane (internal standard), 16.5 mL hexane, 110 mg catalyst, 20 h. The carbon mass balance was in all cases >95%.

2.6.2. Products Selectivity

Chang and co-workers described the evolution of products selectivities as a function of time over the H-BEA catalyst and found that the selectivity to *p*-xylene increases in an almost linear fashion with the increasing time/conversion and so does the selectivity to 2,5-hexanedione. The selectivity to hexanedione, however, starts to decrease as a result of hexanedione being converted back to DMF when certain DMF conversion is reached (60%) [9]. As it can be seen from Figure 7, hexanedione selectivity starts to decline in our case at 40–50% DMF conversion to get dehydrated back to DMF to be converted to *p*-xylene. It can be seen from Figures 8 and 9 that at 180 °C the S(*p*-xylene) increased with increasing conversion only for PZ30 (43.2%) to Z30.2 (44.1%), while it decreased in all other cases of both Z30 and Z80.

It was suggested that this decrease in selectivity to *p*-xylene could be caused by the retention of formed *p*-xylene on acid sites, which would react further to alkylated products (AP) and higher aromatics (HA), which further react to form unrecoverable polymerised products (coke) [32]. However, quantum mechanics calculations showed both hexanedione and oxanorbornene intermediate adsorb stronger (ca. 25.8 kcal/mol) to the acid site as compared with DMF (17.9 kcal/mol) and *p*-xylene (16.6 kcal/mol) [12]. Oxanorbornene can be dehydrated by Brønsted acid sites, as it has been demonstrated by several authors [7,33]; however, Lewis acid sites can be active for the dehydration step as well [13,15,34]. As the adsorbed 7-oxabicyclo[2.2.1]hept-2-ene intermediate can be easily transformed into *p*-xylene, DMF and hexanedione were indicated as the most probable causes for the formation of oligomeric byproducts.

2.6.3. Increasing the Reaction Temperature and Catalyst Reusability

Z80 was chosen as a representative for testing at higher temperatures (Figure 10). Even after the significant conversion increases for Z80.2 (51%) vs PZ80 (16%), S(*p*-xylene) is still higher than

at lower conversion (PZ80) in this case, which further corroborates the hypothesis that the higher reaction temperature is beneficial for the prevention of the unwanted oxanorbornene intermediate reactivity to alkylation and condensation byproducts. Furthermore, the behaviour of Z80.2 at the same temperature of 250 °C but at lower pressure ethylene was tested (Table S1, entries 8, 9). It shows that both the conversion of DMF and *S(p-xylene)* drop almost to the reactivity of the parent PZ80 when lower ethylene pressure is used. This supports the hypothesis that high pressure of ethylene is needed to increase the probability of the cycloaddition step as it was also suggested by Nikbin and co-workers [7].

We also carried out a catalyst reusability test with Z80.2 to investigate how the catalyst performs in repeated tests (Table 3).

Table 3. Catalyst Z80.2 reusability results in the Diels–Alder cycloaddition of 2,5-dimethylfuran and ethylene. Reaction conditions: 220 °C, 55 bar total pressure, 1100 rpm, 2 h reaction time, DMF (12 mL), tridecane (0.98 mL), dodecane (25 mL), 180 mg of Z80.2.

Test Description	X	<i>S(p-Xylene)</i>	S(HDO)	S(MCP)	S(AP)	S(HA)	Carbon Mass Balance
fresh	42.9	50.1	13.9	0.8	16.0	19.2	93.2
reuse 1 *	41.4	51.6	13.7	0.5	17.9	16.3	95.5
reuse 2	42.4	48.8	14.5	0.6	16.0	20.2	92.6
reuse 3	41.7	48.9	14.7	0.5	14.8	21.2	94.6

* catalyst only washed and dried catalyst before the test, catalyst for further reuses (2, 3) was washed, dried, and calcined at 550 °C for 6 h. X, conversion; HDO, hexanedione; MCP, 3-methyl-2-cyclopentenone; AP, alkylated products; and HA, higher aromatics.

It can be seen that the catalyst is reusable without the loss of activity in three subsequent reuses. Also, it should be noted that before the first reuse, the catalyst (pale brown colour) was only washed and dried and still performed similarly to the fresh catalyst (white colour) and last two reuses (white catalyst colour).

2.6.4. Mesoporosity vs Acidity

Both Brønsted [14,35] and Lewis [13,16,34,36] acid sites were shown to be suitable for tandem Diels–Alder cycloaddition of furanic compounds and ethylene [3,18,37]. According to calculations, Brønsted acidity was proven to be more effective than Lewis in the dehydration of the oxanorbornene intermediate [18]. We found that the conversion of DMF per Lewis acid site linearly increased with the increase in the mesopore surface area (Figure 11).

This could mean that as more mesopores are created, the availability of Lewis acid sites increases. We could not find any correlation with Brønsted acid sites, which can be explained either by the Diels–Alder cycloaddition step being rate-determining [18] or also because of the possible synergy between the Brønsted and Lewis sites as it was documented previously [38,39]. In our catalysts, we observed Lewis and Brønsted acid sites and—as the trend of Brønsted acidity was not apparent—the effect of Brønsted acidity was inconclusive. It was suggested in the literature a long time ago that Lewis acids significantly enhance the rate of the Diels–Alder cycloaddition [5,40,41]. However, this depends on the reaction conditions, such as temperature and pressure, as well as concentration of acid sites (high/low), which was shown to affect the regime kinetics [12,13]. As in our case we have dual acidity (Brønsted and Lewis), the most plausible explanation is the enhancement of reactivity by desilication by creating extra-framework Lewis sites (as documented by NMR) with better accessibility, whereas the role of the Brønsted acid sites deserves further investigation.

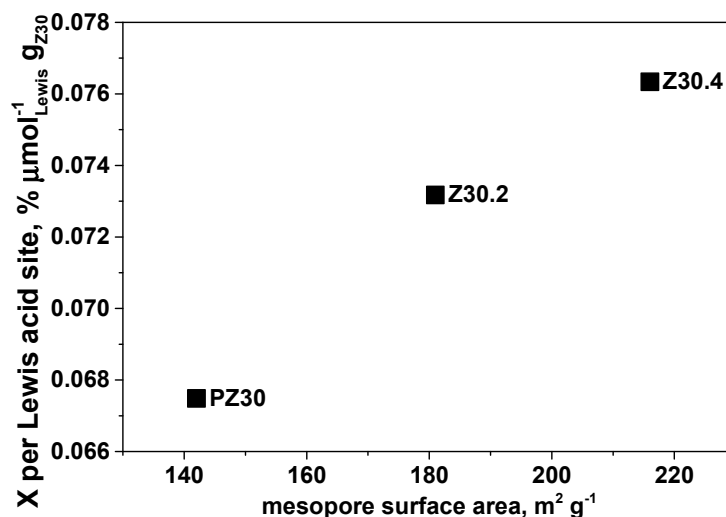


Figure 11. Conversion per Lewis acid site for untreated and treated Z30 vs mesopore surface area for cycloaddition reaction of DMF with ethylene. Reaction conditions: 180 °C, 40 bar total pressure (pressurised at 180 °C), 5.5 mL DMF, 0.45 mL tridecane (internal standard), 16.5 mL hexane, 110 mg catalyst, 20 h.

PZ30 and PZ80 showed similar conversion of DMF of 19.3% and 21.3% and also similar mesopore surface area of 142 and 131 m² g⁻¹, respectively. Still, PZ30 displayed 51% higher selectivity towards *p*-xylene. We believe that this is due to the fact that PZ30 possesses more strong acid sites than PZ80 (416 vs 278 μmol g⁻¹, respectively). This acidity is required for the dehydration of the cycloadduct intermediate to *p*-xylene (Scheme 1). It is also true that there are more Brønsted/Lewis acid sites in PZ30 (295/286 μmol g⁻¹) vs PZ80 (166/167 μmol g⁻¹), which is expected based on the Si/Al ratio. NH₃-TPD measurements confirm that PZ30 and Z30.4 have almost identical amounts of strong acid sites of 416 and 426 μmol g⁻¹, respectively. However, Z30.4 exhibits a 40% increase in conversion compared to its parent PZ30. We propose that this is a result of the increased mesopore area in Z30.4, which was found to be 52% higher when compared to PZ30 (Table 1). This is also supported in the case of alkaline-treated Z80. PZ80 and Z80.4 showed similar amounts of strong acid sites of 278 and 244 μmol g⁻¹, respectively. At the same time, Z80.4 displayed 66% conversion enhancement in comparison with PZ80. Similarly, Z80.4 possessed double the mesopore surface area of PZ80 (Table 1). The increase in conversion for both treated Z30 and Z80 is likely due to the increase in mesoporosity, which could involve both a) higher tolerance to coke formation than in microporous samples thereby extending catalyst lifetime and b) improved reactants diffusion. Coke tolerance of Z80.2 is supported by the reusability test, where the catalyst with coke deposited (pale brown colour) performed the same as the fresh catalyst (white colour) (Table 3).

3. Materials and Methods

3.1. Materials

Commercial ZSM-5 (MFI) zeolites were obtained in the ammonium form (CBV 3024E, SiO₂/Al₂O₃ = 30 and CBV 8014, SiO₂/Al₂O₃ = 80) from Zeolyst International Inc. (Conshohocken, PA, USA). 2,5-dimethylfuran (99%), ammonium nitrate, and tridecane were obtained from Sigma Aldrich (St. Louis, MO, USA). Sodium hydroxide pellets and hexane were obtained from Fisher Scientific (Hampton, NH, USA), and apart from DMF, were used without further purification. DMF was purified by vacuum distillation.

3.2. Catalyst Preparation

Conventional ZSM-5. The ammonium form of ZSM-5 was treated at 550 °C in static air at a heating ramp of 1 °C min⁻¹ for 6 h to produce the proton form of the same material. This was repeated for subsequent calcinations. The parent samples are noted as P (e.g., PZ30).

Alkaline treated ZSM-5. The alkaline-treated ZSM-5 samples are noted according to the amount of NaOH used (e.g., Z30.2 and Z30.4 for 0.2 M NaOH and 0.4 M NaOH treatment of Z30, respectively). The desilication procedure was performed by treating the ammonium form of the zeolite with aqueous sodium hydroxide (30 mL g⁻¹). The mixture was stirred for 30 min at 65 °C and then quenched in an ice bath to prevent further desilication. The slurry was filtered using Whatman grade 3 filter paper. The sample was washed and then dried overnight. The desilicated catalyst was converted to the ammonium form by treating the sample with 1 M ammonium nitrate for 120 min at 80 °C (20 mL g⁻¹). The suspension was cooled, then filtered and dried overnight. Finally, the zeolite was converted from the ammonium into the proton form by calcination as described above.

3.3. Catalytic Activity

DMF was distilled beforehand to remove heavy contaminants, leaving behind a brown residue. The reaction of 2,5-DMF and ethylene was carried out in a 45 mL closed Parr model 4717 pressure reactor. DMF (5.5 mL), tridecane (0.45 mL), hexane (16.5 mL), and 110 mg of catalyst were charged into the vessel. The vessel was stirred using a cross-shaped magnetic stir bar at 1100 rpm, purged with nitrogen, and heated to 180 °C using an aluminium block and a hotplate. As soon as the vessel reached the required temperature, the vessel was pressurised to a total pressure of 40 bar with ethylene for 20 h. At the end of the reaction, the vessel was quenched in an ice bath. The liquid phase was separated from the spent catalyst by centrifugation. Product identification was carried out using gas chromatography (Agilent series 7820A, HP-5 capillary column, 30 m, 0.32 mm, 0.25 µm) (Agilent Technologies, Santa Clara, CA, USA) using flame ionisation detector. The conversion and selectivities were calculated based on the below equations:

$$\text{Conversion}_{\text{DMF}} (\%) = \frac{[\text{DMF}]_{\text{initial}} - [\text{DMF}]_{\text{end}}}{[\text{DMF}]_{\text{initial}}} \times 100$$

$$\text{Selectivity}_{\text{product}} (\%) = \frac{[\text{product}]}{\text{sum of } [\text{products}]} \times 100$$

Carbon mass balance was a sum of concentrations of all identified products and unreacted DMF. Reusability tests were performed with Z80.2 at the following reaction conditions. DMF (12 mL), tridecane (0.98 mL), dodecane (25 mL), and 180 mg of Z80.2 were added to a 75 mL stainless-steel vessel and purged with nitrogen. The vessel was heated to 220 °C and pressurised to a total pressure of 55 bar with ethylene. The reaction was carried out and stirred at 1100 rpm for 2 h. After the reaction was allowed to cool, the spent catalyst was filtered and washed with ethanol and dried in an oven overnight at 110 °C. The spent catalyst was then calcined as described in Section 3.2. The first reuse test was carried out with only washed and dried catalyst (turned pale brown), whereas the subsequent two reuses were done with catalyst regenerated by calcination.

3.4. Characterisation

X-ray diffraction was carried out using a Panalytical X'Pert PRO HTS X-ray diffractometer (PANalytical, Almelo, The Netherlands) using Cu K α radiation ($\lambda = 0.154$ nm). Data were recorded in the 2 θ range of 5–50°. Scanning electron microscopy (SEM) was carried out using Hitachi S-4800 Field Emission Scanning Electron Microscope (Hitachi, Tokyo, Japan). For ICP-OES measurements, approximately 1 mg of zeolite was sonicated in 1 mL of water until a suspension was obtained. The amount of Si and Al in the suspension was measured and used to calculate the SiO₂/Al₂O₃ ratios. Each value of Si and Al was measured three times and averaged. Nitrogen sorption isotherms

were measured using Micromeritics ASAP 2020 (Micromeritics Instrument Corporation, Norcross, Georgia, USA) at 77 K. The surface area was calculated using the BET equation with the P/P_0 range 0.05–0.30. Total pore volume was taken as a volume at $P/P_0 = 0.99$. The micropore volume was calculated using the NLDFT method up to 2 nm pore size. Mesopore surface area was calculated as the difference between the BET surface area and the micropore volume. Temperature desorption of ammonia (NH_3 -TPD) was carried out using Micromeritics Autochem II 2920 (Micromeritics Instrument Corporation, Norcross, GA, USA) equipped with a thermal conductivity detector. The sample (50 mg) was pre-treated in air at 550 °C at a rate of 5 °C min^{-1} and held for 60 min. Then the gas flow was changed from air to helium and flowed at a rate of 20 $\text{cm}^3 \text{min}^{-1}$ for 20 min. The sample was then cooled to 150 °C. Then, 5% NH_3/He mixture was flowed at a rate of 20 $\text{cm}^3 \text{min}^{-1}$ for 30 min. The gas was changed to helium and flowed at a rate of 20 $\text{cm}^3 \text{min}^{-1}$ for 30 min. For TPD, the sample was heated to 700 °C at a rate of 10 °C min^{-1} . Diffuse reflectance infrared Fourier transform (DRIFT) spectra of catalysts were taken on a Nicolet NEXUS FTIR spectrometer (Thermo Fisher Scientific, Waltham, MA, USA) using powdered catalyst mixtures with KBr. H-ZSM-5 was mixed with KBr in a 4:1 weight ratio. The powder was pre-treated at 150 °C/0.01 kPa for 60 min under vacuum. The sample was dried under a flow of nitrogen. Pyridine was dropped onto the sample. The samples were exposed to pyridine for 60 min and then degassed at 150 °C to remove physisorbed pyridine. The Brønsted (B) and Lewis (L) sites were determined using peak intensities at 1540 cm^{-1} and 1450 cm^{-1} , respectively. ^{27}Al MAS NMR spectra were recorded using a Varian VNMRs spectrometer at 104.2 MHz at room temperature in 4 mm rotor with a spinning rate of 14,000 Hz with “onepul” pulse sequence, direct excitation, 1 μs pulse duration, 10 ms acquisition time, 200 ms recycle time, collected 7000 transients, spectral width 416.7 kHz.

4. Conclusions

We have demonstrated that alkaline treatment of H-ZSM-5 is beneficial for the [4 + 2] Diels–Alder cycloaddition of DMF and ethylene when compared to the untreated parent. The alkaline treatment results in the preferential silicon dissolution, which leads to enhanced mesoporosity and also increased conversion of DMF. Furthermore, we showed that by tuning the alkaline treatment one can produce mesoporosity while preserving the crystallinity of the zeolite. This modification of H-ZSM-5 could be applied to other zeolites for subsequent dehydration reactions involving larger aromatic molecules.

The correlation between the increase of the surface area of the mesopores and activity per Lewis acid site was found, which was caused by the better availability of the extra-framework Lewis acid sites in the desilicated zeolite. However, although no correlation was found for Brønsted acidity, its participation cannot be neglected and deserves further investigation.

Also, elevated temperatures are beneficial to prevent further polymerisation reactions, and increased ethylene pressure can significantly enhance the rate of the cycloaddition reaction step.

Supplementary Materials: The following are available online at <http://www.mdpi.com/2073-4344/8/6/253/s1>, Figure S1: NH_3 -TPD profile (left) and column view of number of acid sites (right) of untreated and treated Z30. Adsorption of NH_3 was performed for 30 min at 150 °C followed by inert flush and TPD up to 700 °C. Columns legend: total acidity (black), weak acid sites (pattern), and strong acid sites (grey), Figure S2: NH_3 -TPD profile (left) and column view of number of acid sites (right) of untreated and treated Z80. Adsorption of NH_3 was performed for 30 min at 150 °C followed by inert flush and TPD up to 700 °C. Columns legend: total acidity (black), weak acid sites (pattern), and strong acid sites (grey), Figure S3: SEM micrographs of PZ30 (A–C) and Z30 (D–F), Figure S4 SEM micrographs of PZ80 (A–C) and Z80.2 (D–F), Table S1: Results of Diels–Alder catalytic testing of DMF and ethylene over untreated and treated H-ZSM-5. Reaction conditions: 5.5 mL DMF, 0.45 mL tridecane (internal standard), 16.5 mL hexane, 110 mg catalyst, 20 h. Conversions and selectivities in %. HDO is 2,5-hexanedione, MCP is 3-methyl-2-cyclopentenone, AP are alkylated products, HA are higher aromatics. The rest is selectivity to unknown products. The carbon mass balance was in all cases >94%.

Author Contributions: Conceptualization, J.A.L.-S. and P.P.; Methodology, J.M. and P.P.; Validation, J.M., L.M., P.P., L.D.V., and J.A.L.-S.; Formal Analysis, J.M.; Investigation, J.M., L.D.V., and L.M.; Resources, J.A.L.-S.; Data Curation, J.M. and P.P.; Original Draft Preparation, J.M.; Review and Editing Manuscript, P.P., L.M., L.D.V., and J.A.L.-S.; Visualization, J.M.; Supervision, J.A.L.-S. and P.P.; Project Administration, J.A.L.-S. and P.P.; Funding Acquisition, J.A.L.-S.

Funding: This research was funded by the Engineering and Physical Sciences Research Council (EPSRC) grant number EP/K014773/1. Liqaa Majdal wishes to acknowledge funding of this research by the Higher Committee for Education Development in Iraq.

Acknowledgments: The authors thank Ivan Kozhevnikov's group especially Hossein Bayahia for their help with the FTIR-pyridine measurements and Rob Clowes for his help with the BET measurements. The authors would also like to thank David Apperley for the measurement of solid-state NMR spectra, which were obtained at the EPSRC UK National Solid-State NMR Service at Durham. The authors acknowledge the staff and use of the MicroBioRefinery facility (financed by the Department of Business Skills and Innovation (Regional Growth Fund), where all the experiments were performed.

Conflicts of Interest: The authors declare no conflict of interest. The funding sponsors had no role in the design of the study; in the collection, analyses, or interpretation of data; in the writing of the manuscript; or in the decision to publish the results.

References

1. Lin, Z.; Ierapetritou, M.; Nikolakis, V. Aromatics from lignocellulosic biomass: Economic analysis of the production of p-xylene from 5-hydroxymethylfurfural. *AIChE J.* **2013**, *59*, 2079–2087. [[CrossRef](#)]
2. Maneffa, A.; Priece, P.; Lopez-Sanchez, J.A. Biomass-derived renewable aromatics: Selective routes and outlook for p-xylene commercialisation. *ChemSusChem* **2016**, *9*, 2736–2748. [[CrossRef](#)] [[PubMed](#)]
3. Settle, A.E.; Berstis, L.; Rorrer, N.A.; Roman-Leshkov, Y.; Beckham, G.T.; Richards, R.M.; Vardon, D.R. Heterogeneous diels-alder catalysis for biomass-derived aromatic compounds. *Green Chem.* **2017**, *19*, 3468–3492. [[CrossRef](#)]
4. Cheng, Y.T.; Huber, G.W. Production of targeted aromatics by using diels-alder classes of reactions with furans and olefins over zsm-5. *Green Chem.* **2012**, *14*, 3114–3125. [[CrossRef](#)]
5. Brion, F. On the lewis acid catalyzed diels-alder reaction of furan. Regio- and stereospecific synthesis of substituted cyclohexenols and cyclohexadienols. *Tetrahedron Lett.* **1982**, *23*, 5299–5302. [[CrossRef](#)]
6. Williams, C.L.; Chang, C.C.; Do, P.; Nikbin, N.; Caratzoulas, S.; Vlachos, D.G.; Lobo, R.F.; Fan, W.; Dauenhauer, P.J. Cycloaddition of biomass-derived furans for catalytic production of renewable p-xylene. *ACS Catal.* **2012**, *2*, 935–939. [[CrossRef](#)]
7. Nikbin, N.; Do, P.T.; Caratzoulas, S.; Lobo, R.F.; Dauenhauer, P.J.; Vlachos, D.G. A dft study of the acid-catalyzed conversion of 2,5-dimethylfuran and ethylene to p-xylene. *J. Catal.* **2013**, *297*, 35–43. [[CrossRef](#)]
8. Shiramizu, M.; Toste, F.D. On the diels-alder approach to solely biomass-derived polyethylene terephthalate (pet): Conversion of 2,5-dimethylfuran and acrolein into p-xylene. *Chem.-Eur. J.* **2011**, *17*, 12452–12457. [[CrossRef](#)] [[PubMed](#)]
9. Chang, C.C.; Green, S.K.; Williams, C.L.; Dauenhauer, P.J.; Fan, W. Ultra-selective cycloaddition of dimethylfuran for renewable p-xylene with h-bea. *Green Chem.* **2014**, *16*, 585–588. [[CrossRef](#)]
10. Brandvold, T. Carbohydrate Route to Para-Xylene and Terephthalic Acid. U.S. Patent 8,314,267, 20 November 2012.
11. Roman-Leshkov, Y.; Barrett, C.J.; Liu, Z.Y.; Dumesic, J.A. Production of dimethylfuran for liquid fuels from biomass-derived carbohydrates. *Nature* **2007**, *447*, U982–U985. [[CrossRef](#)] [[PubMed](#)]
12. Patet, R.E.; Nikbin, N.; Williams, C.L.; Green, S.K.; Chang, C.-C.; Fan, W.; Caratzoulas, S.; Dauenhauer, P.J.; Vlachos, D.G. Kinetic regime change in the tandem dehydrative aromatization of furan diels-alder products. *ACS Catal.* **2015**, *5*, 2367–2375. [[CrossRef](#)]
13. Rohling, R.Y.; Uslamin, E.; Zijlstra, B.; Tranca, I.C.; Pilot, I.A.W.; Hensen, E.J.M.; Pidko, E.A. An active alkali-exchanged faujasite catalyst for p-xylene production via the one-pot diels-alder cycloaddition/dehydration reaction of 2,5-dimethylfuran with ethylene. *ACS Catal.* **2018**, *8*, 760–769. [[CrossRef](#)] [[PubMed](#)]
14. Kim, J.-C.; Kim, T.-W.; Kim, Y.; Ryoo, R.; Jeong, S.-Y.; Kim, C.-U. Mesoporous mfi zeolites as high performance catalysts for diels-alder cycloaddition of bio-derived dimethylfuran and ethylene to renewable p-xylene. *Appl. Catal. B Environ.* **2017**, *206*, 490–500. [[CrossRef](#)]
15. Patet, R.E.; Caratzoulas, S.; Vlachos, D.G. Tandem aromatization of oxygenated furans by framework zinc in zeolites. A computational study. *J. Phys. Chem. C* **2017**, *121*, 22178–22186. [[CrossRef](#)]

16. Patet, R.E.; Fan, W.; Vlachos, D.G.; Caratzoulas, S. Tandem diels–alder reaction of dimethylfuran and ethylene and dehydration to para-xylene catalyzed by zeotypic lewis acids. *ChemCatChem* **2017**, *9*, 2523–2535. [[CrossRef](#)]
17. Wijaya, Y.P.; Suh, D.J.; Jae, J. Production of renewable p-xylene from 2,5-dimethylfuran via diels-alder cycloaddition and dehydrative aromatization reactions over silica-alumina aerogel catalysts. *Catal. Commun.* **2015**, *70*, 12–16. [[CrossRef](#)]
18. Nikbin, N.; Feng, S.; Caratzoulas, S.; Vlachos, D.G. P-xylene formation by dehydrative aromatization of a diels–alder product in lewis and brønsted acidic zeolites. *J. Phys. Chem. C* **2014**, *118*, 24415–24424. [[CrossRef](#)]
19. Williams, C.L. Production of Sustainable Aromatics from Biorenewable Furans. Doctoral Dissertations, University of Massachusetts, Amherst, MA, USA, 2014.
20. Moliner, M.; Martinez, C.; Corma, A. Multipore zeolites: Synthesis and catalytic applications. *Angew. Chem. Int. Ed.* **2015**, *54*, 3560–3579. [[CrossRef](#)] [[PubMed](#)]
21. Kim, J.; Choi, M.; Ryoo, R. Effect of mesoporosity against the deactivation of mfi zeolite catalyst during the methanol-to-hydrocarbon conversion process. *J. Catal.* **2010**, *269*, 219–228. [[CrossRef](#)]
22. Groen, J.C.; Peffer, L.A.A.; Moulijn, J.A.; Perez-Ramirez, J. Mesoporosity development in zsm-5 zeolite upon optimized desilication conditions in alkaline medium. *Colloid Surf. A* **2004**, *241*, 53–58. [[CrossRef](#)]
23. Dean, A.Y. Hydrocarbon Conversion Process and Catalyst Comprising a Crystalline Alumino-Silicate Leached with Sodium Hydroxide. US3326797 A, 20 June 1967.
24. Verboekend, D.; Perez-Ramirez, J. Design of hierarchical zeolite catalysts by desilication. *Catal. Sci. Technol.* **2011**, *1*, 879–890. [[CrossRef](#)]
25. Groen, J.C.; Moulijn, J.A.; Perez-Ramirez, J. Decoupling mesoporosity formation and acidity modification in zsm-5 zeolites by sequential desilication-dealuminum. *Microporous Mesoporous Mater.* **2005**, *87*, 153–161. [[CrossRef](#)]
26. Brunner, E.; Pfeifer, H.; Auroux, A.; Lercher, J.; Jentys, A.; Brait, A.; Garrone, E.; Fajula, F. *Acidity and Basicity*; Springer: Berlin/Heidelberg, Germany, 2008.
27. Rodriguez-Gonzalez, L.; Hermes, F.; Bertmer, M.; Rodriguez-Castellon, E.; Jimenez-Lopez, A.; Simon, U. The acid properties of h-zsm-5 as studied by nh₃-tpd and al-27-mas-nmr spectroscopy. *Appl. Catal. A Gen.* **2007**, *328*, 174–182. [[CrossRef](#)]
28. Rac, V.; Rakic, V.; Miladinovic, Z.; Stosic, D.; Auroux, A. Influence of the desilication process on the acidity of hzsm-5 zeolite. *Thermochim. Acta* **2013**, *567*, 73–78. [[CrossRef](#)]
29. Sadowska, K.; Wach, A.; Olejniczak, Z.; Kustrowski, P.; Datka, J. Hierarchic zeolites: Zeolite zsm-5 desilicated with naoh and naoh/tetrabutylamine hydroxide. *Microporous Mesoporous Mater.* **2013**, *167*, 82–88. [[CrossRef](#)]
30. Jiang, Y.J.; Huang, J.; Dai, W.L.; Hunger, M. Solid-state nuclear magnetic resonance investigations of the nature, property, and activity of acid sites on solid catalysts. *Solid State Nucl. Mag.* **2011**, *39*, 116–141. [[CrossRef](#)] [[PubMed](#)]
31. Sklenak, S.; Dedecek, J.; Li, C.; Wichterlova, B.; Gabova, V.; Sierka, M.; Sauer, J. Aluminium siting in the zsm-5 framework by combination of high resolution al-27 nmr and dft/mm calculations. *Phys. Chem. Chem. Phys.* **2009**, *11*, 1237–1247. [[CrossRef](#)] [[PubMed](#)]
32. Do, P.T.M.; McAtee, J.R.; Watson, D.A.; Lobo, R.F. Elucidation of diels-alder reaction network of 2,5-dimethylfuran and ethylene on hy zeolite catalyst. *ACS Catal.* **2013**, *3*, 41–46. [[CrossRef](#)] [[PubMed](#)]
33. Salavati-fard, T.; Caratzoulas, S.; Doren, D.J. Solvent effects in acid-catalyzed dehydration of the diels-alder cycloadduct between 2,5-dimethylfuran and maleic anhydride. *Chem. Phys.* **2017**, *485–486*, 118–124. [[CrossRef](#)]
34. Chang, C.-C.; Je Cho, H.; Yu, J.; Gorte, R.J.; Gulbinski, J.; Dauenhauer, P.; Fan, W. Lewis acid zeolites for tandem diels-alder cycloaddition and dehydration of biomass-derived dimethylfuran and ethylene to renewable p-xylene. *Green Chem.* **2016**, *18*, 1368–1376. [[CrossRef](#)]
35. Li, Y.-P.; Head-Gordon, M.; Bell, A.T. Computational study of p-xylene synthesis from ethylene and 2,5-dimethylfuran catalyzed by h-bea. *J. Phys. Chem. C* **2014**, *118*, 22090–22095. [[CrossRef](#)]
36. Wijaya, Y.P.; Kristianto, I.; Lee, H.; Jae, J. Production of renewable toluene from biomass-derived furans via diels-alder and dehydration reactions: A comparative study of lewis acid catalysts. *Fuel* **2016**, *182*, 588–596. [[CrossRef](#)]

37. Fan, W.; Cho, H.J.; Ren, L.; Vattipailli, V.; Yeh, Y.-H.; Gould, N.G.; Xu, B.; Gorte, R.J.; Lobo, R.; Dauenhauer, P.J.; et al. Renewable p-xylene from 2,5-dimethylfuran and ethylene using phosphorus-containing zeolite catalysts. *ChemCatChem* **2016**. [[CrossRef](#)]
38. Yu, Z.; Li, S.; Wang, Q.; Zheng, A.; Jun, X.; Chen, L.; Deng, F. Brønsted/lewis acid synergy in h-zsm-5 and h-mor zeolites studied by ¹h and ²⁷al dq-mas solid-state nmr spectroscopy. *J. Phys. Chem. C* **2011**, *115*, 22320–22327. [[CrossRef](#)]
39. Zheng, A.; Li, S.; Liu, S.-B.; Deng, F. Acidic properties and structure–activity correlations of solid acid catalysts revealed by solid-state nmr spectroscopy. *Acc. Chem. Res.* **2016**, *49*, 655–663. [[CrossRef](#)] [[PubMed](#)]
40. Houk, K.N.; Strozier, R.W. Lewis acid catalysis of diels-alder reactions. *J. Am. Chem. Soc.* **1973**, *95*, 4094–4096. [[CrossRef](#)]
41. Birney, D.M.; Houk, K.N. Transition structures of the lewis acid-catalyzed diels-alder reaction of butadiene with acrolein—The origins of selectivity. *J. Am. Chem. Soc.* **1990**, *112*, 4127–4133. [[CrossRef](#)]



© 2018 by the authors. Licensee MDPI, Basel, Switzerland. This article is an open access article distributed under the terms and conditions of the Creative Commons Attribution (CC BY) license (<http://creativecommons.org/licenses/by/4.0/>).